The Journal of Experimental Biology **199**, 1931–1946 (1996)
Printed in Great Britain © The Company of Biologists Limited 1996
JEB0098

DYNAMICS AND ENERGETICS OF SCALLOP LOCOMOTION

J.-Y. CHENG*, I. G. DAVISON† AND M. E. DEMONT‡
Department of Biology, Saint Francis Xavier University, PO Box 5000, Antigonish, Nova Scotia, Canada B2G 2W5

Accepted 24 May 1996

Summary

A dynamic model for a swimming scallop was developed which integrates the mechanical properties of the hinge ligaments, valve inertia, the external fluid-flow reaction, the fluid pressure in the mantle cavity and the muscle contraction. Kinematic data were recorded for a swimming *Placopecten magellanicus* from high-speed film analysis. Dynamic loading experiments were performed to provide the required mechanical properties of the hinge for the same species. The swimming dynamics and energetics based on data from a 0.065 m long *Placopecten magellanicus* at 10 °C were analyzed. The main conclusions are as follows.

1. The mean period of a clapping cycle during swimming is about 0.28 s, which can be roughly divided into three equal intervals: closing, gliding and opening. The maximum angular velocity and acceleration of the valve movements are about 182 degrees s^{-1} and 1370 degrees s^{-2}, respectively.

2. The hysteresis loop of the hinge was found to be close to an ellipse. This may be represented as a simple Voigt body consisting of a spring and dashpot in parallel, with a rotational stiffness of 0.0497 N m and viscosity coefficient of 0.00109 kg m^2 s^{-1} for the 0.065 m long *Placopecten magellanicus*.

3. The external fluid reaction has three components, of which the added mass is about 10 times higher than the mass of a single valve, and the flow-induced pseudo-viscosity compensates for nearly half of the hinge viscosity for the 0.065 m long *Placopecten magellanicus*.

4. The locomotor system powered by the muscle can be divided into two subsystems: a pressure pump for jet production and a shell-hinge/outer-fluid oscillator which drives the pumping cycle. The dynamics of the oscillator is determined predominantly by the interaction of the external fluid reaction and the hinge properties, and its resonant frequency was found to be close to the swimming frequencies.

5. The momentum and energy required to run the oscillator are negligibly small (about 1 % for the 0.065 m long *Placopecten magellanicus*) compared with that for the jet. Almost all the mechanical energy from muscle contraction is used to perform hydrodynamic work for jet production. Thus, the Froude efficiency of propulsion in scallops is nearly the same as the entire mechanical efficiency of the locomotor system. This could be a fundamental advantage of jet propulsion, at least for a scallop.

6. The estimated maximum muscle stress is about 1.06×10^5 N m^{-2}, the cyclic work is 0.065 J and power output is 1.3 W. Using an estimate of the mass of an adductor muscle, the work done by the muscle per unit mass is 9.0 J kg^{-1} and the peak power per unit mass is 185 W kg^{-1}.

7. The time course of the force generation of the contracting adductor muscle is basically the same as that of the hydrodynamic propulsive force.

Key words: swimming, jet propulsion, kinematics, dynamics, energetics, muscle, hydrodynamic forces, viscoelasticity, scallop, *Placopecten magellanicus*.

Introduction

Locomotion of most aquatic animals is achieved by interaction of the body with the surrounding fluid and is powered by the contraction of muscles. The cyclic motion of the body parts or appendages results in a fluid reaction on the animal, which is in the direction of swimming and balances both the drag and the weight. The mechanical energy generated by the muscles not only contributes to the hydrodynamic work but also powers the reciprocal movements of the locomotor apparatus. Studies of the dynamics and energetics of aquatic locomotion must include all of the important mechanical elements associated with the swimming animal, such as the fluid dynamic reaction, the body inertia, the response of deformed tissues and the muscle contraction. Studies that integrate these elements must be based on suitable mechanical and morphological analyses.

Such an integrative approach has been explored recently for

*Present address: Drill Bit Engineering, Smith International, Inc., 16740 Hardy Street, PO Box 60068, Houston, TX 77205-0068, USA.
†Present address: Department of Biological Sciences, Simon Fraser University, Burnaby, British Columbia, Canada V5X 1S6.
‡Author for correspondence.

swimming in some aquatic vertebrates and invertebrates (DeMont and Gosline, 1988; Daniel *et al.* 1992; DeMont, 1992; Bowtell and Williams, 1994; Cheng and Blickhan, 1994). Obviously, integration is possible and reliable only after a detailed understanding of each mechanical component has been obtained. In each of these studies, however, more accurate data were needed or some important mechanism was not considered. In this paper, we examine the locomotion of the scallop *Placopecten magellanicus*. The simple locomotory system of this animal allowed us to perform a relatively complete mechanical analysis.

Scallop swimming, with the ventral side foremost through the water, is produced by jets of water from two openings near the hinge (Trueman, 1975; Gould, 1971; Moore and Trueman, 1971; Gruffydd, 1976; Morton, 1980; Vogel, 1985; Dadswell and Weihs, 1990; Hayami, 1991). Contraction of the adductor muscle closes the two valves of the scallop and ejects water. Valve opening is basically powered by the release of strain energy stored in the hinge ligaments during valve closing.

There have been previous reports on the mechanical components of scallop swimming. The mechanical properties of the hinge ligaments in scallops have been evaluated for various species (Alexander, 1966; Vogel, 1985; DeMont, 1990; Bowie *et al.* 1993; Fung, 1993). DeMont (1990) developed a model to examine a possible resonant phenomenon in the swimming scallop system. Marsh *et al.* (1992) studied the *in vivo* mechanical performance of a scallop adductor muscle during natural swimming by measuring the pressure power of fluid in the mantle cavity, the hinge power and the acceleration power. The contractile and mechanical properties of the striated adductor muscle of *Argopecten irradians* have been studied *in vitro* at different temperatures (Olson and Marsh, 1993). Marsh and Olson (1994) measured the *in vitro* performance of muscles under *in vivo* strain cycle conditions.

The mechanical performance of locomotion is determined by the interaction of all of the mechanical elements in the system. In previous studies on scallop locomotion, some of these mechanical elements were omitted or incorrectly modelled. In particular, the unsteady fluid reaction on the clapping valves due to the flow around the outer surface of the valves was not correctly considered. We have recently completed an analysis on these unsteady fluid forces (Cheng and DeMont, 1996*a*). In the present paper, a dynamic model for a swimming scallop was developed using a more complete description of all relevant mechanical elements. These include the fluid loading from the flow outside the valves and from the flow within the mantle cavity during jetting, the properties of the hinge, the shell inertia and the muscle contraction. The locomotor system was modelled as two subsystems: a pressure pump for jet production and a shell-hinge/outer-fluid oscillator to accomplish the pumping cycle. Complete kinematic data were recorded using high-speed cine film analysis. The viscoelastic properties of the hinge were measured during dynamic loading experiments. The fluid pressure in the mantle cavity was obtained using an approach based on a fluid-mechanics analysis of the flow in the cavity and through the orifices. This dynamic analysis is based on kinematic data from free-swimming animals and does not utilize invasive procedures, such as measurements of mantle pressure using cannulae or telemetery (Webber and O'Dor, 1986; Marsh *et al.* 1992). The dynamic behaviour of the locomotor system and the flow of energy from the contraction of the adductor muscle of a 0.065 m long *Placopecten magellanicus* swimming at 10 °C are presented in this paper. The present approach can also be used to infer the *in vivo* force behaviour of the striated muscle during natural locomotion, which will be given elsewhere.

Materials and methods

We first present tests on the mechanical properties of the hinge, following which the collection of kinematic data on scallop swimming is described. A fluid-mechanics analysis is then given for calculation of the reaction due to the fluid pressure in the mantle cavity based on kinematic and morphometric data. Finally, a dynamic model of the locomotor system is developed by combining all the mechanical elements associated with swimming which were developed in the previous sections.

Mechanical properties of the hinge

The hinge consists of the inner (abductin) and outer ligaments. The mechanical properties of the hinge ligaments have been studied for *Pecten maximus* and *Chlamys opercularis* (Alexander, 1966; DeMont, 1990) and *Argopecten irradians* (Vogel, 1985). In those studies, the static rotational stiffness of the inner hinge ligaments was measured. Bowie *et al.* (1993) measured the resilience of the oscillating hinge for *Placopecten magellanicus* and found it to be approximately 90 % at physiological frequencies and environmental temperatures. This indicates that there is an energy loss, although not large, associated with the dynamic behaviour of the viscoelastic materials of the hinge. To model the constitutive relationship of the scallop hinge quantitatively, we carried out dynamic loading experiments on the hinge.

Scallops, *Placopecten magellanicus* (Gmelin), ranging in mass from 0.024 to 0.121 kg and in shell height (distance from the hinge to the front of the animal, see Fig. 2) from 0.038 to 0.104 m, were obtained from the Department of Fisheries and Oceans, Halifax, Nova Scotia, Canada, and were maintained at 10 °C in a 370 l recirculating tank filled with sea water. They were maintained according to the guidelines of the Canadian Council for Animal Care. The scallops were eviscerated, and the sides were trimmed from both valves to reduce total mass and therefore inertial error in the measurements. The shells were fastened to a servo-system apparatus (Cambridge Technology model 310) using a nut passed through a small hole drilled into the bottom valve. The upper valve was left to move freely, and the servo-system arm rested on the top of this valve approximately

0.01 m from the ventral tip. A signal generator (Hewlett-Packard 8904A) was used to drive the servo arm, and therefore the valve, in a sine wave at frequencies ranging from 0.5 to 5.0 Hz in steps of 0.5 Hz. The amplitude of the sine wave was set to simulate an *in vivo* displacement of the valves. The displacement of the valve and its upward force on the servo arm were recorded using a digitizing oscilloscope (Hewlett-Packard 54501A) and a microcomputer (Gateway 4DX2/50) and were converted to SI units. The temperature was maintained at 10±0.5 °C by performing the test in a small refrigerator (Kenmore), and sea water was dripped over the hinge using a peristaltic pump (Omega) to keep it from drying out during the trial.

The force–displacement curve for the hinge of a 0.063 m long animal oscillated at 3 Hz is shown in Fig. 1. The shape of the hysteresis loop of the hinge is very close to an ellipse; thus, the scallop hinge can be modeled as a Voigt body consisting of a spring and dashpot in parallel. The elastic and viscous coefficients of the Voigt body can be determined by measuring the slope and area of the hysteresis loop (Thomson, 1988). From the data obtained at a forcing frequency of 3 Hz (Fig. 1), which is close to the natural swimming frequency, the rotational stiffness (k_h) and viscous coefficient (c_h) of the hinge can be measured as:

$$k_h = 49.69\times10^{-3}\ \mathrm{N\,m}, \quad (1)$$

$$c_h = 1.09\times10^{-3}\ \mathrm{kg\,m^2\,s^{-1}}. \quad (2)$$

The general mechanical behaviour of the hinge is then described by:

$$M_h = k_h\gamma + c_h\frac{d\gamma}{dt}, \quad (3)$$

where M_h is the moment about the hinge (in N m), t is time and γ is the angular displacement of the hinge (in degrees). Using the model (equation 3) with the measured values of k_h and c_h, we can obtain the variation of the force with the displacement cycle, which replicates the cycle used in the loading experiments. The force–displacement curve obtained from equation 3 is also plotted in Fig. 1 (Voigt body line), which shows that the model approximates the viscoelastic properties of the hinge quite well. A more complete analysis of the hinge mechanics, including the effects of temperature, will be presented elsewhere.

Kinematic analysis

Several scallops were placed in a 370 l recirculating tank at 10 °C with a thin layer of sand on the bottom and filled with sea water. The tank was illuminated by two 1000 W tungsten spot/flood lamps (Ianebeam 1000), placed approximately 0.8 m away from the scallops. One side of the tank contained a large glass window through which filming took place, and a white-on-black grid with 0.02 m spacing was placed on the rear of the tank for distance calibration on the film. A starfish (*Asterias forbesii*), a natural predator of the scallop, was placed on the rear of the scallop, causing it either to take flight or to open and close its shell in a single clap. When this happened, the scallop was filmed using a high-speed cine

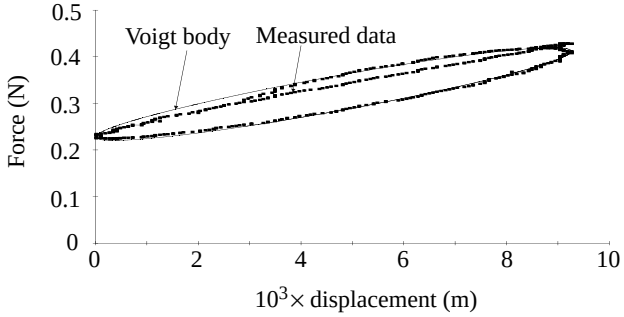

Fig. 1. The force–displacement curve for a hinge isolated from a 0.063 m long scallop and oscillated at a frequency of 3 Hz. The force was measured at a location approximately 0.010 m away from the ventral tip, where the distance between the two shells followed a sinusoidal cycle with the amplitude simulating the values during swimming. The hysteresis loop of the Voigt body used to model the hinge properties is also shown (solid line).

camera (Red Lake Laboratories Locam, Kern Vario-Switar Compact lens) at 300 frames s^{-1} (nominal camera setting), placed 1–1.5 m away from the tank. In all cases, the movement of the animal was well aligned with the plane of the film. The camera was started as soon as the scallop moved on the bottom of the tank, so that by the time the animal entered the field of view, the camera was up to speed. After development, the film (Kodak Eastman 7250) was projected onto a white screen, magnifying the image of the scallop by about a factor of 5, and played frame-by-frame. The shell height S_L was measured (to ±0.2 cm on the projected image) in the first frame, and the gape (distance between the top and bottom valves at the front of the animal) was measured in each frame (to ±0.2 cm on the projected image). This allowed calculation of the angle of opening [$\gamma(t)=\sin^{-1}(\mathrm{gape}/S_L)$] between the two valves at each time interval (given by the frame speed of the camera), so that angle of shell opening *versus* time could be plotted.

The magnification of the projected image was approximately 5.6, which is considered to be large enough to reduce the error in high-speed filming (Harper and Blake, 1989). The kinematic data were treated by using a spline software package GCVSPL, which has been used previously to analyze fish swimming (Beddow *et al.* 1995) and in many biomechanics studies. The angle *versus* time data were smoothed and interpolated with a quintic spline function using GCVSPL. This package was chosen because it offers reliable estimation of higher derivatives. The velocity and acceleration are the first and second derivatives of the smoothing spline function. In GCVSPL, the amount of smoothing required for specific data is determined by several statistical considerations (Woltring, 1986), which can be used to determine the spline coefficients iteratively. The four given choices for smoothing were tested on our data. The so-called true predicted mean-squared error (MSE) criteria was used in our data analysis.

Theoretical models

Hydromechanical analysis of the flow in the mantle cavity

While the valves are closing, water in the cavity is ejected

from two orifices near the hinge. There is thus a time-dependent force acting on the inner surfaces of the two shells due to the fluid pressure of the jet flow. The adductor muscle pulls the two valves against this fluid force, which can be calculated from a simple fluid-mechanics analysis and the kinematic data. It is assumed that the fluid in the cavity is inviscid and that there is no energy dissipation when water goes through the orifices. When the jets are well formed at the orifices, the exit area is very small compared with the shell area, and the steady Bernoulli equation can be used to model the flow in the mantle cavity and through the opening. Along a streamline connecting a point at the inner surface of the shell and a point at the exit, we have:

$$p_s + \frac{1}{2}\rho U_s^2 = p_j + \frac{1}{2}\rho U_j^2, \quad (4)$$

where p_s, p_j and U_s, U_j are the pressure and velocity at the shell and exit, respectively, and ρ is the density of sea water. Since the movements of the two shells are assumed to be symmetrical about an average plane (commissural plane) (see Fig. 3), the gravitational term has been ignored in the above equation. If the total gape angle is $\gamma(t)$ at any instant, the oscillation of either shell can be described by $\beta(t)=\gamma(t)/2$. According to the non-penetration condition, the velocity (U_s) of a fluid particle adjacent to the shell at position S_x (Fig. 2) is equal to the velocity of the shell at the same position, i.e.:

$$U_s = -S_x \frac{d\beta(t)}{dt}, \quad (5)$$

and is normal to the shell surface. Denoting A_j as the cross-sectional area of the jet, which can be time-dependent during the jetting phase, A_v as the valve area, A_m as the cross-sectional area of the adductor muscle and S_L as the shell height (Fig. 2), the averaged jet velocity over the cross section of the jet at the orifice (U_j) can be obtained from the mass conservation law as (Cheng and DeMont, 1996*b*):

$$U_j = \frac{\lambda_A}{2\lambda_{Aj}} S_L \frac{d\beta(t)}{dt}, \quad (6)$$

where $\lambda_A=1-(A_m/A_v)$ and $\lambda_{Aj}=A_j/A_v$. The pressure at the exit is reasonably approximated by the fluid pressure at infinity. So, from equation 4, the effective pressure at the inner surface of the shell (p_i) is:

$$p_i = p_s - p_j = \frac{1}{2}\rho S_L^2 \left[\left(\frac{\lambda_A}{2\lambda_{Aj}}\right)^2 - \left(\frac{S_x}{S_L}\right)^2\right]\left(\frac{d\beta}{dt}\right)^2, \quad (7)$$

which may be simplified to:

$$p_i = p_{i\beta}(S_x)\left(\frac{d\beta}{dt}\right)^2. \quad (8)$$

This equation is obtained from the mass conservation and the momentum theorem of fluid flow. It gives a relationship between the fluid pressure at the inner surface of the shell, the valve closing velocity, the jet area and geometrical parameters. Note that the pressure is not constant in the cavity (equation 4) and over the shell (equation 7). In many studies on aquatic jet propulsion, the fluid pressure was only measured at one point in the mantle cavity (Trueman, 1975; Webber and O'Dor, 1986; DeMont and Gosline, 1988; O'Dor, 1988; Marsh *et al.* 1992). Strictly speaking, the pressure is not uniform in the cavity: the value is close to ambient near the orifice and is higher at a position away from the exit. If the reading is taken at some point where a mean value over the valve cavity can be obtained, the resulting estimation of the jet energy or jet thrust may be close to the real case, as long as other relevant data are available. The energy required to form the internal flow that is eventually ejected from the orifices is an integral sum of the distributive quantities over the whole cavity surface. In general, more attention should be paid to the measurement of pressure in studies on jet propulsion. Nevertheless, it can be verified that, if the jet opening is much smaller than the surface

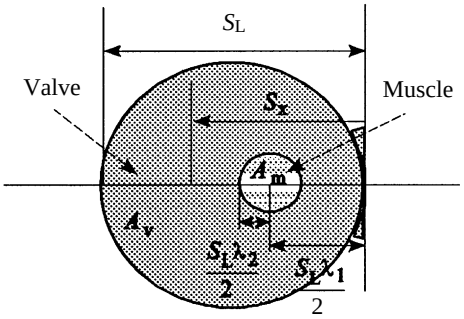

Fig. 2. Schematic top view of a scallop, showing the parameters used to describe its morphology. A_v is the area of the valve projected on the commissural plane, A_m is the cross-sectional area of the adductor muscle, S_L is the shell height, S_x is the *x*-coordinate of any position on the shell, $S_L\lambda_1/2$ is the distance normal from the hinge to the centre of the muscle, and $S_L\lambda_2/2$ is the radius of the muscle.

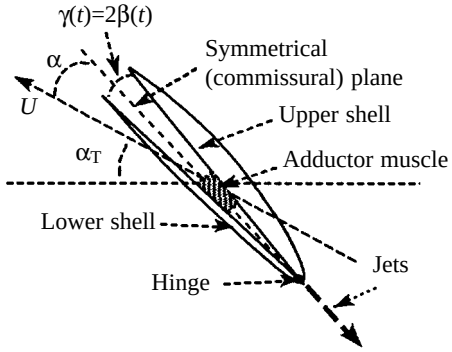

Fig. 3. Schematic side (anterior) view of a swimming scallop. The gape angle $\gamma(t)=2\beta(t)$ is used to describe the opening and closing of the shell around the hinge. α is the angle of attack between the swimming direction and the mean plane of the two shells, and α_T is the trajectory angle between the swimming direction and horizontal surface. U is the swimming speed.

area of the cavity, the fluid particle velocity at the cavity wall (U_s) is much lower than the averaged jet speed (U_j) and then the pressure may be approximated as uniform. We found this to be true for a scallop, after examining equation 7 using appropriate morphometric data. However, during the initial part of the adduction, the mantle velum around the valve does not seal completely, which results in a large opening. The power calculated from the assumption of a uniform pressure measured at one point could then be rather inaccurate, and therefore we will use equation 7 to calculate the pressure distribution on the shell.

The total force due to the inner fluid pressure acting on, for example, the upper shell (F_{fi}) (excluding the part occupied by the adductor muscle) is (positive in the direction of shell opening):

$$F_{fi}(t) = \iint_{A_v - A_m} p_i(S_x)\mathrm{d}A = F_{fi\beta}\left(\frac{\mathrm{d}\beta}{\mathrm{d}t}\right)^2, \tag{9}$$

$$F_{fi\beta} = \frac{1}{8}\rho\pi S_L{}^4\left\{\left(\frac{\lambda_A}{2\lambda_{Aj}}\right)^2(1-\lambda_2{}^2) - \frac{1}{4}\left[\frac{5}{4} - \lambda_2{}^2\left(\lambda_1{}^2 + \frac{\lambda_2{}^2}{4}\right)\right]\right\}, \tag{10}$$

where λ_1 and λ_2 are determined by the position and cross-sectional size of the muscle connecting the two shells, and A_v–A_m is the integral domain (Fig. 2).

The moment about the hinge due to the inner fluid pressure acting on the upper shell (M_{fi}) is (positive in the clockwise direction):

$$M_{fi}(t) = \iint_{A_v - A_m} p_i(S_x)(-S_x)\mathrm{d}A = M_{fi\beta}\left(\frac{\mathrm{d}\beta}{\mathrm{d}t}\right)^2, \tag{11}$$

$$M_{fi\beta} = M_{fi\beta 0} + M_{fi\beta 1} = \frac{1}{64}\rho\pi S_L{}^5\left\{\left[\left(\frac{\lambda_A}{\lambda_{Aj}}\right)^2(1-\lambda_1\lambda_2{}^2)\right] + \left[\lambda_1\lambda_2{}^2\left(\lambda_1{}^2 + 3\frac{\lambda_2{}^2}{4}\right) - \frac{7}{4}\right]\right\}, \tag{12}$$

where $M_{fi\beta 0}$ is the moment constant due to the uniform pressure distribution and $M_{fi\beta 1}$ is the moment constant due to the contribution of the variable pressure.

The moment M_{fi} (or force F_{fi}) is proportional to the square of the valve angular velocity, which varies during adduction. It should be mentioned that, in general, the jet area A_j (or λ_{Aj}) can be time-dependent during jetting. However, the quantification of the variation of the jet area is difficult. Our observations (Cheng and DeMont, 1996*b*) suggest that jet size is fairly constant for the well-formed jet which appears during most of the jetting phase. A constant jet area (see Table 2) is therefore used in our numerical calculations, but the equations presented above can be used for more general cases for which the variable jet area is recorded.

There is also an inward flow through the gape between the valves during abduction. In principle, the same approach as above can be taken to find the fluid pressure distribution in the cavity in relation to the variation in gape angle. The mantle velum regulates the flow through the ventral mantle margin, but its control is not precisely known. Thus, the area of the opening cannot be easily determined at any instant in time. However, this problem is not important: since the animal is immersed in an infinite fluid medium and the opening is towards the swimming direction, the cavity is probably filled instantly while the shells are opening. Thus, only a very low pressure difference (negative effective pressure) will be needed to draw water into the cavity, as was measured by Marsh *et al.* (1992). Therefore, the moment (or force) due to the inner fluid pressure during the abduction will be omitted in our present model, since it is negligibly small compared with the moment during the adduction.

The integrated dynamic model and energy expenditure

Scallops rotate the two shells around the hinge during swimming. The rapid closing of the two valves is caused by the nearly simultaneous contraction of the entire striated adductor muscle (Marsh *et al.* 1992), which is directly attached to the valves (Fig. 3). Abduction of the valves is powered by the strain energy stored in the hinge ligaments during valve closure. The production of the propulsive jet is the result of the high fluid pressure in the mantle cavity generated by the shells during contraction of the adductor muscles. The periodic motion of the shells is also subject to the time-dependent reaction of the outer flow around the swimming scallop.

The dynamic system of the swimming scallop can be represented by the model shown in Fig. 4A, in which the rectilinear displacement of the mass element (shell) is equivalent to the angular displacement. Note that the spring and dashpot arranged in parallel represent the hinge, in accordance with the results given above. Since the motion of two shells is viewed as symmetrical with respect to the average (commissural) plane, the system can be further separated into two subsystems which function equally. Hence, we only need to consider, for example, the upper shell movement (Fig. 4B). In Fig. 4B, I_v is the inertial moment of half of the two-valve mass, and k_h and c_h are the rotational effective stiffness and damping coefficient of the hinge, respectively. M_{fi} and M_{fe} are the fluid dynamic moments of the internal and external flow about the hinge, respectively. It is a system with one degree of freedom. If we assume that the hinge ligaments are basically in compression throughout the cycle, the momentum equation can immediately be written as (positive in the clockwise direction):

$$I_v\frac{\mathrm{d}^2\beta(t)}{\mathrm{d}t^2} = M_m - 2c_h\frac{\mathrm{d}\beta(t)}{\mathrm{d}t} - 2k_h[\beta(t) - \beta_{max}] + M_{fi} + M_{fe}, \tag{13}$$

where M_m is the total moment produced by muscle contraction, and β_{max} is the maximum half-gape angle. The moment caused

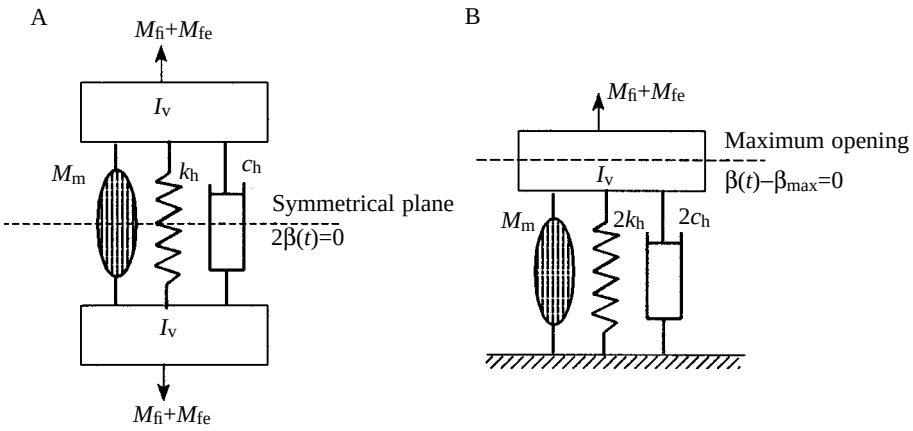

Fig. 4. (A) The dynamic model of a swimming scallop. The hinge is represented by a spring with rotational stiffness k_h and a dashpot with damping coefficient c_h in parallel, as discussed in the text. The two shells are represented by the two mass elements (each with an inertial moment of I_v), each of which experiences a hydrodynamic moment exerted by the outer fluid flow (M_{fe}) and a hydrodynamic moment due to the fluid pressure in the mantle cavity (M_{fi}). The rectilinear displacement of the mass element (or shell) is equivalent to the angular displacement. The symmetrical (commissural) plane is the mean plane of the two shells at any instant. The adductor muscle pulls the two shells together during the jetting phase, generating a total moment M_m, and the hinge resilience pushes them apart during the opening phase. (B) The dynamic system for the upper shell, which is equivalent to the dynamic model shown in A (see text). Note that the coefficients of viscosity and stiffness are doubled. β_{max} is the maximum half-gape angle; $2\beta(t)$ is the gape angle.

by the external fluid reaction (M_{fe}) is (Cheng and DeMont 1996*a*):

$$M_{fe} = -I_f \frac{d^2\beta(t)}{dt^2} + c_f \frac{d\beta(t)}{dt} + k_f\beta(t), \quad (14)$$

where

$$I_f = \frac{17}{60\pi}\rho S_L^5, \quad (15)$$

$$c_f = \frac{1}{2\pi}\rho U S_L^4, \quad (16)$$

and

$$k_f = \frac{1}{3\pi}\rho U^2 S_L^3. \quad (17)$$

The meaning of the three terms, i.e. the added moment of inertia of one shell, I_f, the rotational viscous coefficient of pseudo-viscosity c_f, and the rotational pseudo-stiffness k_f, have been discussed previously (Cheng and DeMont, 1996*a*). It is clear that the outer fluid reaction is not represented only by the added-mass effect. Generally, a phase shift exists between the hydrodynamic force and the displacement (or acceleration), which may play an important role in coordinating aquatic locomotion, as has already been shown for fish swimming (Lighthill, 1975; Cheng *et al.* 1991; Blickhan and Cheng, 1994). The moment due to the inner jetting flow is given by equation 11. Substituting equations 11 and 14 into equation 13 yields:

$$I\frac{d^2\beta(t)}{dt^2} + c\frac{d\beta(t)}{dt} + k\beta(t) - M_{fi\beta}\left[\frac{d\beta(t)}{dt}\right]^2 - 2k_h\beta_{max} = M_m, \quad (18)$$

where

$$I = I_v + I_f, \quad (19)$$

$$c = 2c_h - c_f, \quad (20)$$

and

$$k = 2k_h - k_f, \quad (21)$$

are the effective inertial moment (I), viscous coefficient (c) and stiffness (k) due to the hinge and outer fluid reaction, respectively. The outer fluid reaction will reduce the effects of the mechanical stiffness and damping of the scallop hinge.

The dynamic swimming system may conveniently be divided into two sub-elements: the jet pump and the oscillator, consisting of the shell, hinge and outer fluid. The force generated by the muscle contraction is used partly to pump fluid and partly to excite the shell-hinge/outer-fluid oscillator. The oscillator system works throughout the entire cycle, while the pump only works during part of the cycle. Suppose the part of the total muscle moment used to run the oscillator is M_{mo} and the remaining part used to produce the jet flow is M_{mj}. Then we have:

$$M_m = M_{mo} + M_{mj}, \quad (22)$$

$$M_{mo} = I\frac{d^2\beta(t)}{dt^2} + c\frac{d\beta(t)}{dt} + k\beta(t) - 2k_h\beta_{max}, \quad (23)$$

$$M_{mj} = -M_{fi\beta}\left[\frac{d\beta(t)}{dt}\right]^2, \; t \in \Delta t_c, \quad (24)$$

where M_{mj} is generated during the valve closing time interval (Δt_c), but does not exist during the remaining part of the cycle. The passive muscle force is very low compared with the active force (Olson and Marsh, 1993). It can be speculated that most of the muscle force will be used to produce the jets, i.e. M_{mj} is much larger than M_{mo}: this will be shown later.

Suppose that the pulling force of the contracting muscle is uniformly distributed over the cross section of the adductor, the muscle stress σ can then be estimated from the muscle moment as:

$$\sigma = 2\frac{M_m}{S_L\lambda_1 A_{mq}}, \; t \in \Delta t_c, \quad (25)$$

where $S_L\lambda_1/2$ is the distance between the hinge and the centre of the cross section of the muscle (Fig. 2), and A_{mq} is the cross-sectional area of the fast part of the adductor muscle.

The strain of the adductor muscle ε can be defined as:

$$\varepsilon = \frac{L_{mo} - L_m}{L_{mo}}, \tag{26}$$

where L_{mo} is the muscle length at the centre of the cross section when the valves are at the maximum opening during swimming, and L_m is the muscle length at any instant. The muscle length when the valves are completely closed, L_{mc}, is:

$$L_{mc} = t_m - t_s, \tag{27}$$

where t_m is the thickness of the aerofoil shape of the scallop and t_s is the thickness of the two shells. Since

$$L_{mo} = L_{mc} + \beta_{max} S_L \lambda_1, \tag{28}$$

and

$$L_m = L_{mc} + \beta(t) S_L \lambda_1, \tag{29}$$

from equation 26, the strain is then:

$$\varepsilon = \frac{\beta_{max} S_L \lambda_1}{L_{mc} + \beta_{max} S_L \lambda_1} - \frac{S_L \lambda_1}{L_{mc} + \beta_{max} S_L \lambda_1} \beta(t) = \varepsilon_0 - \varepsilon_1 \beta(t), \tag{30}$$

where ε_0 and ε_1 are defined by the first and second terms, respectively. The strain rate of the adductor muscle is:

$$\frac{d\varepsilon}{dt} = -\varepsilon_1 \frac{d\beta(t)}{dt}. \tag{31}$$

Based on equations 25, 30 and 31, the stress–strain and stress–strain rate relationships can be constructed for the contracting adductor muscle of a scallop during swimming.

The total power generated by the muscle contraction, P_m, is the sum of the power spent on the jets, P_{mj}, and the power for the oscillator, P_{mo}:

$$P_m = M_m \left(2 \frac{d\beta}{dt}\right) = P_{mo} + P_{mj}, \tag{32}$$

where

$$P_{mj} = -2 M_{fi\beta} \left(\frac{d\beta}{dt}\right)^3 = P_{mj0} + P_{mj1}, \tag{33}$$

$$P_{mo} = P_k + P_d + P_e = 2 \left[I \frac{d\beta}{dt} \frac{d^2\beta}{dt^2} + c \left(\frac{d\beta}{dt}\right)^2 + k\beta \frac{d\beta}{dt} \right], \tag{34}$$

where P_k is the rate of change of kinetic energy for the scallop shell mass and added mass, P_d is the rate of energy dissipation by the effective damping and P_e is the rate of change of the strain energy stored in the effective spring. P_{mj0} and P_{mj1} from equation 33 are defined as:

$$P_{mj0} = -2 M_{fi\beta 0} \left(\frac{d\beta}{dt}\right)^3, \tag{35}$$

and

$$P_{mj1} = -2 M_{fi\beta 1} \left(\frac{d\beta}{dt}\right)^2, \tag{36}$$

where $M_{fi\beta 0}$ and $M_{fi\beta 1}$ can be calculated from equation 12. It can easily be verified that P_{mj0} due to the uniform pressure (equation 11) is exactly the flux rate of the fluid kinetic energy of the ejected jets, i.e. the hydrodynamic power of the jets, which has been widely used in many previous studies. The jet power due to the variable pressure, P_{mj1}, was found to be much lower than P_{mj0} and can be neglected for scallops.

The work done by the muscle during one cycle W_m is therefore:

$$W_m \int_T P_m dt = W_{mj} + W_{mo} = -2 M_{fi\beta} \int_T \left(\frac{d\beta}{dt}\right)^3 dt + 2c \int_T \left(\frac{d\beta}{dt}\right)^2 dt, \tag{37}$$

where W_{mo} and W_{mj} are the work on the oscillator and jets, respectively, and T is the time for one cycle. The power and work per unit mass can be obtained by dividing the above quantities by the mass of the adductor muscle.

If the moment (force) generated by muscle contraction during natural swimming is known, the movement of the shells can be predicted by solving equations 22–24. Measurements of muscle force during natural swimming are currently difficult to obtain for scallops or any other living animals (Alexander, 1992). However, the problem can be reversed, and the dynamic equations presented here can be used to infer the *in vivo* muscle performance and the energetics of the locomotor system from the measured kinematic data if the mechanics of all passive dynamic elements in the system are known. We investigated the dynamic properties of the scallop swimming system, muscle performance and mechanical energy cost in natural swimming using data from *Placopecten magellanicus*.

Results

Kinematics

Five swimming sequences were recorded from three individuals. The animals swam approximately parallel to the grid plane in each sequence. Because scallops are not active swimmers and the field of view of the camera was very limited, swimming events could not be recorded easily. Most filmed events consisted of climbing before level swimming was achieved. Fig. 5A gives the variation in gape angle with time for a 0.065 m long animal. In the GCVSPL software package, a trade-off between the smoothness of the spline (or of its *m*th derivatives) and the goodness-of-fit to the given data can be modified by varying a parameter called VAL. The measured data and smoothed data at VAL=1, 3 and 10 under the MSE criteria are shown in Fig. 5. Increasing VAL increases the smoothness of the spline (Fig. 5A) and its derivatives (Fig. 5B,C), but reduces the goodness-of-fit as indicated by the variance, VAR. Three spline functions at VAL=1, 3 and 10 give obviously different results. The differences in the acceleration curves (Fig. 5C) are especially significant. The curve at VAL=1 gives the highest value at the maximum

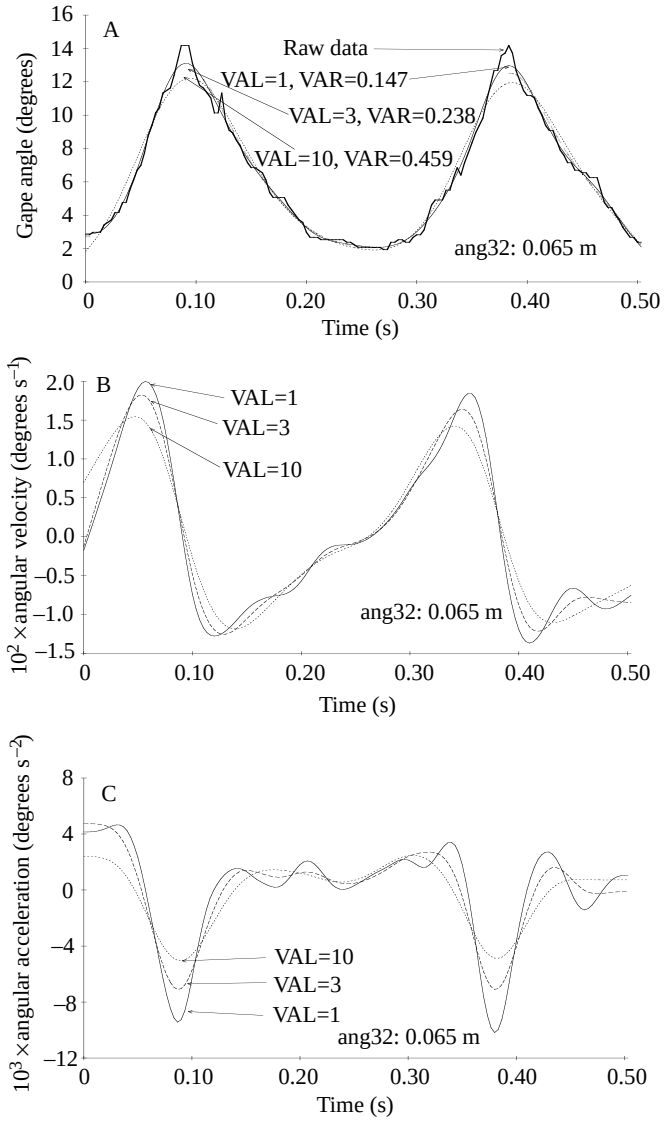

Fig. 5. Comparison of the kinematic data before and after spline smoothing for a scallop of 0.065 m in height (ang32). (A) Gape angle, showing both raw data and the data smoothed using the GCVSPL spline method at VAL=1, 3 and 10 (see text). (B) Angular velocity at VAL=1, 3 and 10. (C) Angular acceleration at VAL=1, 3 and 10. VAR is the variance of the spline smoothing.

acceleration, but shows serious fluctuations during the remaining part of one period, which is an artefact of the analysis. The spline at VAL=10 gives relatively smooth accelerations but the lowest maximum value, which could be an underestimate. The problem of choosing a suitable smoothness to obtain the most accurate acceleration may be resolved only by using other measurement methods, such as an accelerometer (Harper and Blake, 1989). We decided to use the spline function with MSE at VAL=3 to analyse our kinematic data, since it gives a fairly good general behaviour in angular acceleration and a reasonable estimation of maximum acceleration for scallop swimming.

The gape angle displacements, angular velocities and

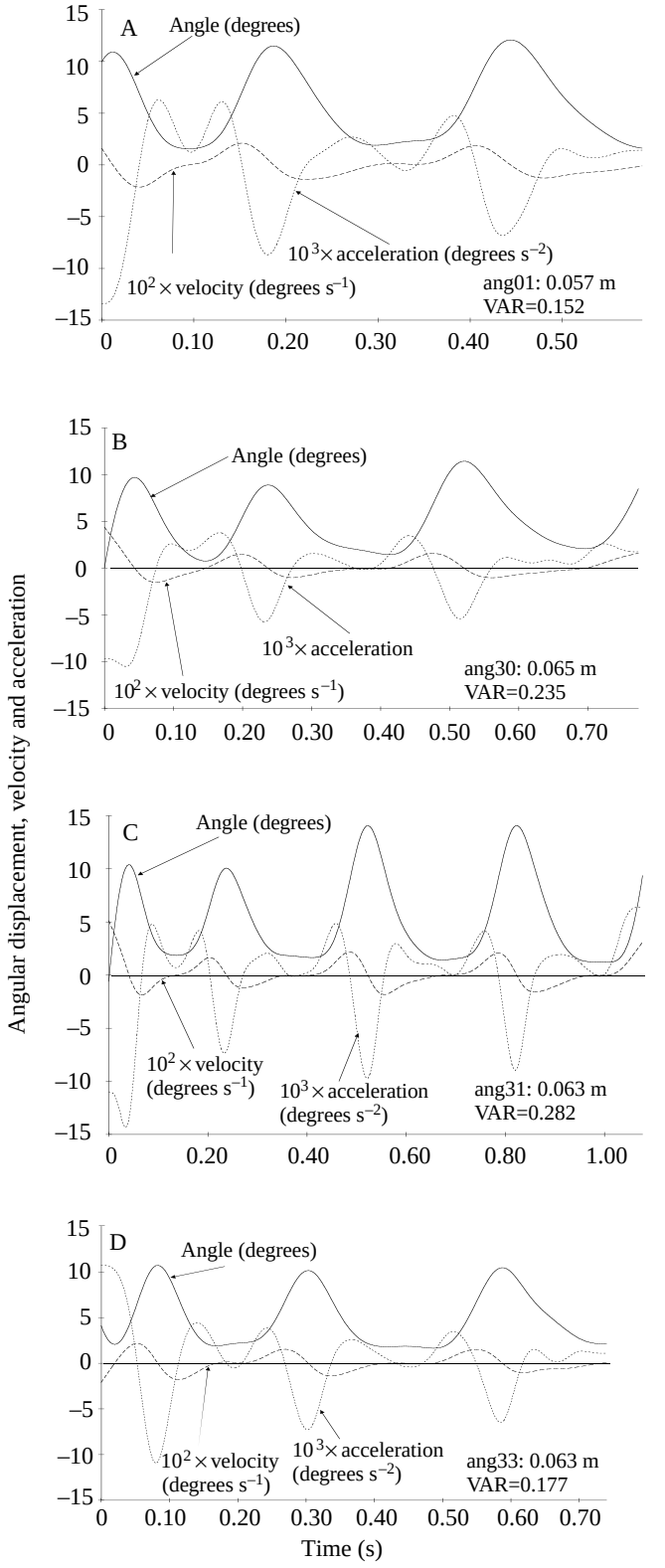

Fig. 6. Variation in gape angle, angular velocity and angular acceleration with time during four swimming sequences. All data were smoothed using the GCVSPL spline method with VAL=3. VAR is the variance of the spline smoothing. (A) An individual with a shell height of 0.057 m (ang01); (B) 0.065 m (ang30); (C) 0.063 m (ang31); (D) 0.063 m (ang33).

accelerations of four swimming sequences are shown in Fig. 6A–D. The data were smoothed using GCVSPL with MSE criteria and VAL=3. It was found that the shell movement is not harmonic, although it is periodic. A remarkable gliding phase, during which the valves are closed, was observed for all sequences. The angular displacement curves of the opening and closing phases are approximately symmetrical about the maximum value of the angle, which indicates that the duration of opening is very close to that of closing. The velocity increases as the shells open and reaches a maximum at about one-third of the maximum angle, decreasing to zero at the maximum opening angle. As the shells close, the angular velocity becomes more negative and reaches the maximum closing value, after which it becomes less negative, gradually approaching zero after the shells are closed. A constant angular velocity during shell closing has been assumed in almost all studies on aquatic jet propulsion in scallops and other jet-propelled animals. From our measurements, this is approximately true only for the middle one-third of the closing duration. In general, however, the angular velocity is not constant during the shell closing phase. Maximum acceleration occurs just before maximum gape angle is reached. Fluctuations in acceleration values around and during the gliding phase are considered to be artefacts, as discussed earlier.

For descriptive purposes, it is convenient to subdivide the time period T of one clapping cycle into three intervals. (1) The opening phase, $\Delta t_o=\lambda_{to}T$, during which the half-gape angle increases from zero to a maximum (β_{max}). (2) The closing phase, $\Delta t_c=\lambda_{tc}T$, during which the half-gape angle decreases from β_{max} to zero. (3) The gliding phase, $\Delta t_g=\lambda_{tg}T$, during which the valves are kept closed or move only very slowly, where $\lambda_{to}+\lambda_{tc}+\lambda_{tg}=1$.

Table 1 lists the maximum and minimum gape angles, maximum opening and closing velocities and the maximum absolute accelerations from one typical period for all five swimming sequences. The complete period is taken from the last maximum opening angle to the previous maximum opening angle of the valves. Approximate values of the average closing angular velocities and the durations of the closing, gliding and opening phases are also given in Table 1. The mean swimming speed and the trajectory angle with respect to the horizontal surface (see Fig. 3) were obtained for three sequences.

Dynamics of the locomotor system

The dynamics analysis is based on one swimming sequence: ang32 (see Table 1; Fig. 5) for a 0.065 m long *Placopecten magellanicus*. Results for the other swimming sequences were similar and are not shown for brevity. The kinematic data and morphometric parameters used to calculate the parameters in the dynamics equation are listed in Table 2. The volume of the expellable water in the mantle cavity V_e is equal to the volume enclosed by the mantle velum and the two planes connecting the edges of the shells, V_s, minus that of the adductor muscle, V_m. The latter (V_m) depends on the location of the adductor, which varies during ontogeny (Gould, 1971; Dadswell and Weihs, 1990). Thus, the expellable volume at any instant is:

$$V_e = V_s - V_m = \lambda_A A_v S_L \beta , \tag{38}$$

where

$$\lambda_A = \frac{A_v - \lambda_1 A_m}{A_v} = 1 - \lambda_1 \lambda_2{}^2 . \tag{39}$$

$S_L\lambda_1/2$, $S_L\lambda_2/2$ are shown in Fig. 2. Generally, λ_1 varies during growth and is approximately equal to 1 for the 0.065 m long animal (Dadswell and Weihs, 1990; Table 2).

The resulting dynamic parameters, such as the coefficients of the external forces, the mechanical properties of the hinge and other parameters in the dynamic equations are given in Table 3. Fig. 7A shows the normalized variation in gape angle,

Table 1. *Kinematic data of shell clapping during the swimming escape response of* Placopecten magellanicus *at 10 °C*

	Flight (ang01)	Flight (ang30)	Flight (ang31)	Flight (ang32)	Flight (ang33)
Shell length (m)	0.057	0.065	0.063	0.065	0.063
Δt_c (s)	0.083	0.088	0.092	0.092	0.081
Δt_g (s)	0.086	0.104	0.114	0.11	0.125
Δt_o (s)	0.084	0.088	0.088	0.079	0.082
T (s)	0.253	0.28	0.294	0.281	0.288
γ_{min} (degrees)	1.9	1.45	1.42	2.1	1.64
γ_{max} (degrees)	11.51	8.9	14.1	12.75	10.15
$(d\gamma/dt)_{mo}$ (degrees s^{-1})	1.87×10^2	1.58×10^2	2.08×10^2	1.82×10^2	1.53×10^2
$(d\gamma/dt)_{mc}$ (degrees s^{-1})	-1.4×10^2	-1×10^2	-1.82×10^2	-1.25×10^2	-1.4×10^2
$(d^2\gamma/dt^2)_m$ (degrees s^{-2})	-8.69×10^3	-5.72×10^3	-9.73×10^3	-7.1×10^3	-7.28×10^3
$(d\gamma/dt)_{ac}$ (degrees s^{-1})	-1.15×10^2	-0.81×10^2	-1.37×10^2	-1.14×10^2	-1.04×10^2
U (m s^{-1})		0.28		0.24	0.23
α_T (degrees)		20.6		26.8	25.7

Δt_c, Δt_g, Δt_o and T are the durations of the closing, gliding and opening phases and one clap cycle, respectively; γ_{min}, γ_{max} are the maximum and minimum gape angles; $(d\gamma/dt)_{mo}$, $(d\gamma/dt)_{mc}$, $(d^2\gamma/dt^2)_m$ and $(d\gamma/dt)_{ac}$ are the maximum opening and closing angular velocities, maximum angular acceleration and averaged closing angular velocity, respectively; U is the mean swimming speed; α_T is the trajectory angle (see Fig. 3).

Identification of each sequence is in parentheses.

Table 2. *Kinematic and morphometric data for the dynamic analysis of a swimming scallop* Placopecten magellanicus *at 10 °C*

	Value	Source
Shell height, S_L (m)	0.065	ang32
Period, T (s)	0.29	ang32
Maximum half-gape angle, β_{max} (rad)	0.1112	ang32
Minimum half-gape angle, β_{min} (rad)	0.0183	ang32
Effective maximum half-gape angle, β_{mm} (rad)	0.0929	ang32
Maximum half-angular velocity, $d\beta/dt$ (rad s^{-1})	1.59	ang32
Maximum half-angular acceleration, $d^2\beta/dt^2$ (rad s^{-2})	61.93	ang32
Swimming speed, U (m s^{-1})	0.24	ang32
Position of muscle, $S_L\lambda_1/2$	0.5	DW
Ratio of muscle to valve area, A_m/A_v	0.065	G
λ_1	1	DW
λ_2	0.255	G
$\lambda_A=1-(A_m/A_v)= 1-\lambda_2^2$	0.935	G
$\lambda_{Aj}=A_j/A_v$	0.00971	CD
Thickness of aerofoil for closed valves, t_m (m)	0.01566	DW
Thickness of two shells, t_s (m)	0.001	ang32
Muscle length for closed valves, L_{mc} (m)	0.01466	ang32
Muscle length at maximum opening, L_{mo} (m)	0.0207	ang32
L_{mo}/L_{mc}	1.41	ang32
Maximum strain, ε_0	0.292	ang32
ε_1	3.14	ang32

ang32, swimming sequence given in Table 1; CD, Cheng and DeMont (1996*b*); DW, Dadswell and Weihs (1990); G, Gould (1971).

angular velocity and acceleration with time for the swimming sequence used in the analysis.

The function of the adductor muscle is twofold: first to pump water present in the mantle cavity to form the propulsive jet, and second to run the shell-hinge/outer-fluid subsystem. The latter can be modelled by a common oscillator consisting of a spring, dashpot, mass and exciting source (equation 23). From the parameters in Table 3, the natural frequency f of such an oscillator is:

$$f = \frac{1}{2\pi}\sqrt{\frac{k}{I}} = \frac{1}{2\pi}\sqrt{\frac{2k_h - k_f}{I_v + I_f}} = 4.67\,\text{Hz}. \qquad (40)$$

The clapping frequency of *P. magellanicus* during natural swimming is 3.40–3.95 Hz for the five swimming sequences we recorded and is approximately 2.0 Hz for a 0.050 m long *Argopecten irradians* (Marsh and Olson, 1994) and 4.0 Hz for a 0.052 m long *Chlamys hastata* (Marsh *et al.* 1992). No swimming speeds were given in these studies.

The moments about the hinge due to the three elements in the oscillator, external hydrodynamic forces (M_{fe}), hinge reaction (M_h), valve inertia (M_v) and their sum to be supplied by muscle contraction (M_{mo}) *versus* time are shown in Fig. 7B. The amplitude of M_v is much smaller than those of M_{fe} and M_h. Since M_v is proportional to the angular acceleration, it reaches its peak value when the gape angle is close to the maximum value. The moment due to the external fluid reaction, M_{fe}, is largely dominated by the added-mass effect at this low swimming speed. Thus, the shape of the curve for M_{fe} is close to that of the angular acceleration. The high hinge moment lasts during the gliding phase of the cycle. As the damping of the hinge is very weak compared with the elastic effect, the shape of the M_h curve is close to that of the gape angle with time. Thus, M_h and M_{fe} are approximately out of phase. The resulting muscle moment M_{mo} required to sustain the operation of the shell-hinge/outer-fluid oscillator is determined by the interaction of the external fluid reaction and the hinge properties, with very little contribution from the valve inertia. M_{mo} is negative over the whole cycle. This means that a tensile force is applied over the whole cycle. There are two maximum values during one cycle: one occurs at about the maximum gape angle, and is associated with the peak of the external fluid reaction; the second appears just before valve opening, and is associated with the force applied by the compressed hinge.

The dynamics of the whole locomotor system is shown in Fig. 7C. The magnitude of M_{mo} is very low over the whole cycle, compared with that of M_{mj}, the moment required to make the jets at the two orifices. The curves of M_{mj} and M_m are hardly distinguishable. Thus, the total active muscle moment M_m required to run the whole system is almost completely determined by the jet production. The magnitude of the moment increases sharply when the valves are closing, reaches a peak after one-quarter of the closing phase, and approaches zero at the end of the closing phase.

Power output of adductor muscle and swimming cost

Power is plotted against time in Fig. 7D. The power–time curves of P_m and P_{mj} almost overlap each other. The mechanical power required to move the oscillator is very low. The power output of the adductor muscle is thus largely for jet production. The time course of the total muscle power P_m is very similar to that of the total muscle moment (Fig. 7C,D). It increases rapidly to a peak value when the valves are closing, then drops to zero. This corresponds to a single contraction of the adductor. Except for the absence of an initial peak just before the major peak, our curve of the *in vivo* power output

Table 3. *Dynamic parameters based on data for a 0.065 m long scallop* Placopecten magellanicus *swimming at 10 °C*

Pseudo-stiffness, k_f (N m)	1.713×10^{-3}
Pseudo-viscosity, c_f (kg m^2 s^{-1})	0.695×10^{-3}
Added inertia moment of one shell, I_f (kg m^{-2})	106.79×10^{-6}
Hinge stiffness, k_h (N m)	49.69×10^{-3}
Hinge viscosity, c_h (kg m^2 s^{-1})	1.09×10^{-3}
Valve inertia moment, I_v (kg m^{-2})	9.955×10^{-6}
Effective stiffness, k (N m)	97.667×10^{-3}
Effective viscosity, c (kg m^2 s^{-1})	1.485×10^{-3}
Effective inertia moment, I (kg m^{-2})	116.75×10^{-6}
Coefficient of internal flow moment, $M_{fi\beta}$ (kg m^2)	0.503
Coefficient of muscle stress, σ_{mm} (m^{-3})	0.174×10^{6}
Density of sea water, ρ (kg m^{-3})	1.02×10^{3}

of the scallop is close to that obtained for *Argopecten irradians* by Marsh *et al.* (1992), who used a different approach.

The peak values of the power due to the oscillator, the jet and the whole system are listed in Table 4. Notice that the value of the total power is not simply the sum of those of the subsystems, because there is a phase delay between the two dynamic processes. The averaged power output over the cycle and the work done by the adductor in one cycle are also given in Table 4.

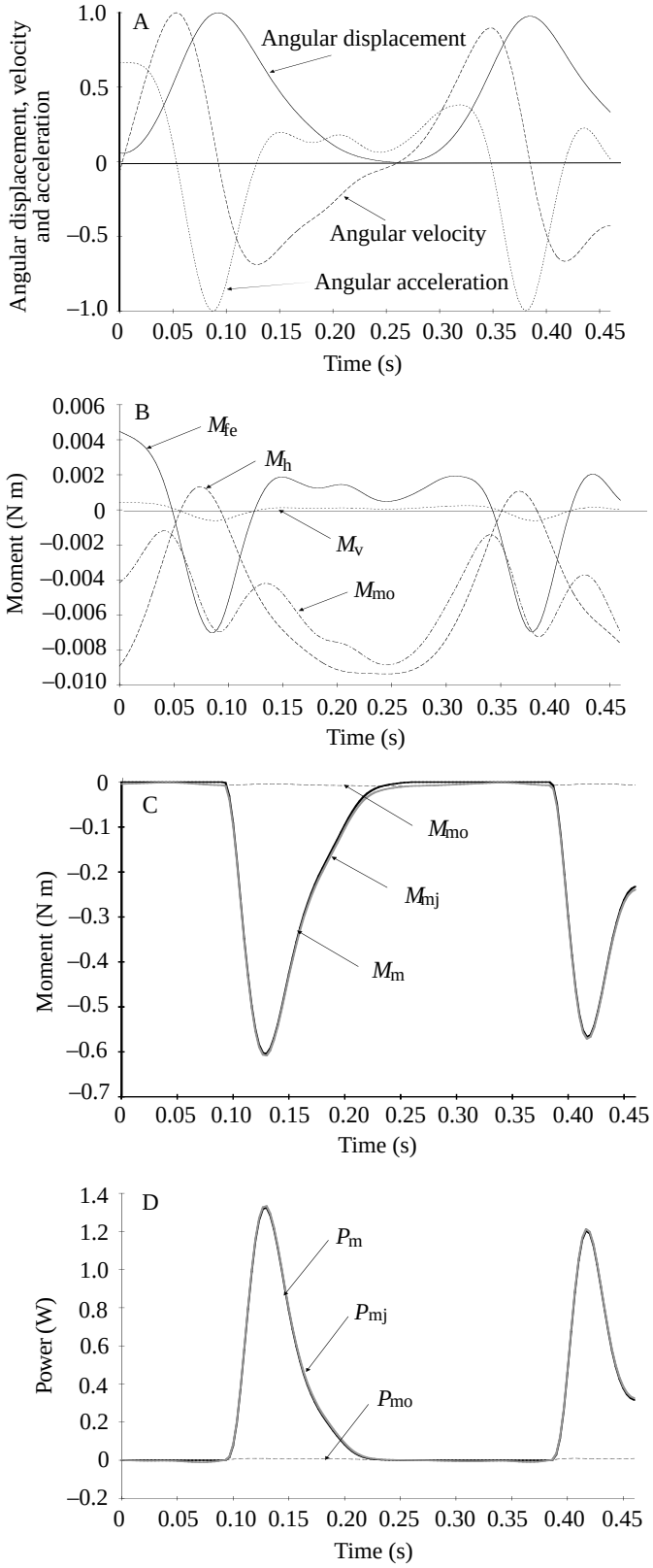

Fig. 7. (A) The variation of the gape angle, angular velocity and angular acceleration with time during one swimming sequence for a 0.065 m long *Placopecten magellanicus* at 10 °C. The curves have been normalized to the maximum angle of gape, the maximum angular velocity or the maximum angular acceleration, respectively. This swimming sequence was used to calculate the dynamic quantities (see text). (B) Moments *versus* time for the dynamic elements in the oscillator. M_{fe} is the moment due to the external fluid reaction, M_h is the moment of the hinge, M_v is the inertial moment of one valve, M_{mo} is the sum of these three and is generated by the muscle to run the subsystem of the oscillator. (C) Moments *versus* time for the entire dynamic system. M_{mj} is the moment required to increase the pressure for the jets, M_{mo} is the moment required to run the subsystem of the oscillator and M_m is the total moment generated by the muscle to operate the whole locomotor system for swimming. (D) Power output *versus* time. P_{mj} is the power required to make the jets, P_{mo} is the power required to run the oscillator and P_m is the total power supplied by the muscle contraction.

Discussion

Kinematics

The period and the amplitude of the clap cycle were variable during each swimming sequence. For most sequences, the clap period increased during swimming. This was caused by the animals climbing from the bottom to a state of level swimming during the filming sessions. The jet force contributes both to support of the body weight and to overcoming the drag. During level swimming, the buoyant body weight will be largely supported by the hydrodynamic lift, and thus the required jet force is reduced (Cheng and DeMont, 1996*b*). The average jet force is proportional to the clapping frequency; thus, the reduced jet force slows the clapping.

The shell oscillation of the scallop in steady swimming is not harmonic (Figs 5, 6). This is different from the steady swimming of most fishes, in which the periodic undulation of the body and caudal fin are quite close to harmonic motion (Videler, 1993). In scallop swimming, one clap cycle can be divided into three phases: closing, gliding and opening. For *Placopecten magellanicus*, the averaged period of one complete clap was approximately 0.28 s, or a frequency of about 3.57 Hz. Shell closing lasts for approximately 0.087 s, and shell opening is a little shorter, about 0.084 s. The gliding phase is the longest, lasting about 0.108 s. During this phase, movement of the two valves is minimized. Since the valves are almost closed, the scallops may be maximizing the hydrodynamic advantage created by their low form drag in this configuration. Nevertheless, the definition of the gliding phase is quite arbitrary. It merely represents a period when the valves move very slowly after the rapid adduction phase and before the rapid abduction phase.

Table 4. *Estimated energetic quantities for a 0.065 m long* Placopecten magellanicus *at 10 °C*

	Oscillator	Jet	Total
Maximum moment (N m)	–0.0089	–0.6041	–0.6084
Peak power (W)	0.0090	1.3242	1.3335
Averaged power (W)			0.2206
Cyclic work (J)	0.502×10^{-3}	64.255×10^{-3}	64.757×10^{-3}
Maximum muscle stress ($N\,m^{-2}$)			0.1059×10^{6}
Maximum strain		0.293	
Maximum strain rate in closing (s^{-1})		3.441	
Maximum strain rate in opening (s^{-1})		–4.486	

The closing speed of the shell reaches a constant maximum value during one-third of the whole closing process and is variable over the remainder. This may be true for other jet-propelled animals, although many studies have assumed a constant ejection speed (Moore and Trueman, 1971; Weihs, 1977; Madin, 1990). As an approximation, and for a more convenient hydrodynamic calculation of the jet propulsive force, a constant closing speed (calculated as the averaged closing speed over the closing phase) can be assumed. For *Placopecten magellanicus*, the mean closing speed is about 75–85 % of the maximum angular speed. The maximum angular velocity was 182 degrees s^{-1}, while maximum angular acceleration occurred at approximately the maximum gape angle and was 1370 degrees s^{-2}.

Swimming dynamics

The external fluid reaction on a swimming scallop has three components: the added-mass effect, flow-induced pseudo-elasticity and pseudo-viscosity. The added-mass force is independent of the swimming speed of the animal, but the pseudo-viscoelasticity force is proportional to the swimming speed (equation 14). During level swimming, a higher mean swimming speed of 0.55 m s^{-1} has been reported (Dadswell and Weihs, 1990). For this swimming speed, the flow induced pseudo-viscoelasticity will have a significant influence on both the amplitude and phase of the hydrodynamic force. The swimming sequences recorded in the present study included climbing, and the main sequence analysed was at a speed of 0.24 m s^{-1}. For this low speed, the hydrodynamic force will be dominated by the added mass, which is about 10 times higher than the valve mass. We have shown that the dynamics of the shell-hinge/outer-fluid subsystem and the muscle force required to sustain the system are largely determined by the interaction of the external fluid reaction and the mechanical response of the hinge.

We have assumed that the hinge ligaments work continuously in compression. The results in Fig. 7B show that the adductor should always provide a tensile force to maintain the momentum balance of the oscillator (negative values of M_{mo} during the whole clapping cycle. Obviously, M_{mo} is supplied by the contraction of the fast part of the adductor muscle during the closing phase. During the gliding and opening phases, the tensile force opposing abduction could be supplied by the action of the smooth part of the adductor. However, such a force will be very small, or zero, if the slow part of the adductor muscle is not active during the gliding and opening phases. We have omitted the tension provided by the relaxed adductor, which is antagonistic to the hinge ligaments and is probably very small (Olson and Marsh, 1993). If the effect of the relaxed adductor is included in the oscillator, the net stiffness of the whole elastic mechanism due to the hinge and adductor should be lower than the values for the hinge ligament alone. This will reduce the magnitude of the hinge moment (M_h). Furthermore, during the gliding and opening phases, the low negative effective fluid pressure which has been omitted in the present model will assist in pulling the valves together. Thus, the magnitude of the calculated muscle moment during gliding, and in particular during the opening phase, will be lower than that shown in Fig. 7B and will probably approach zero.

The oscillator will actually have a lower natural frequency if the stiffness of the relaxed adductor is taken into account for calculation of k_h (see equation 40). The mass or moment of inertia of the shell is proportional to the third power of the shell height (Dadswell and Weihs, 1990). The added inertia is proportional to the fifth power of the shell height, and the pseudo-elastic stiffness (k_f) is proportional to the square of the swimming speed. Thus, the natural frequencies of larger and faster animals will be lower than the calculated value of

Table 5. *Estimated* in vivo *mass-specific muscle performance for* Placopecten magellanicus *and data for* Argopecten irradians *and* Chlamys hastata

	Placopecten	*Argopecten*	*Chlamys*
Peak power ($W\,kg^{-1}$)	185	110–160	120–225
Averaged power ($W\,kg^{-1}$)	30.6	25–33	30–62
Cyclic work ($J\,kg^{-1}$)	9	11–21	8–17

The experimental temperature for all three species was 10 °C. The dorsal–ventral length and the striated muscle mass of the three animals are 0.065 m and 7.21×10^{-3} kg for *Placopecten magellanicus*, 0.0501 m and 1.95×10^{-3} kg for *Argopecten irradians* and 0.052 m and 1.55×10^{-3} kg for *Chlamys hastata*.

Data for *A. irradians* and *C. hastata* are taken from Marsh *et al.* (1992).

4.67 Hz and may be close to the more commonly observed clapping frequency of approximately 3 Hz. Therefore, scallops might be designed to work at near their resonant frequencies to operate the passive oscillator (the shell-hinge/outer-fluid subsystem) more effectively, as already suggested by DeMont (1990).

If the whole locomotor system is considered, the required moment for the oscillator is negligibly low during the closing phase compared with the required moment for jet production (Fig. 7C). During the gliding and opening phases, the fast part of the adductor muscle is not active, i.e. $M_{mj}(t)=0$, where $t=\Delta t_g+\Delta t_o$. The total muscle moment (M_m) is equal to the moment due to the oscillator (M_{mo}), which is determined by the moments of the hinge and by hydrodynamics. The momentum balance is shown in Fig. 7B,C for the gliding and opening phases.

The instantaneous propulsive force F of the two jets is (Cheng and DeMont, 1996*b*):

$$F=\frac{\rho(\lambda_A S_L)^2 A_v}{2\lambda_{Aj}}\left(\frac{d\beta}{dt}\right)^2, \qquad (41)$$

and, from equation 24, we can see that, for any given individual, the thrust differs from the muscle moment for jet production only by a constant coefficient. Therefore, since the muscle moment to run the oscillator can be neglected, the time course of the force generation of the contracting adductor muscle is the same as that of the hydrodynamic propulsive force. The latter determines the swimming performance (Cheng and DeMont, 1996*b*). The maximum thrust occurred at approximately one-quarter of the closing phase, at which point the muscle generates its peak force value. This simple mechanical design and dynamic process of scallop swimming results in a simple control and coordination of locomotion. It is speculated that jet-propelled animals such as squid may use a similar mechanism. Recent studies on fish swimming show that there are complex timing relationships between the contracting force of the muscle distributed along the body and the hydrodynamic propulsive force (Cheng *et al.* 1994).

Although the magnitude of M_{mo} is much smaller than that of M_{mj}, the oscillator is still an important part of the whole locomotor system. Apart from the adductor muscle, the hinge ligaments are some of the key components required to perform clapping. The hinge ligaments should provide sufficient resilience to balance the fluid reaction and shell inertia. This is optimised by tuning the oscillator to near its resonant frequency. The minimum stiffness of the hinge, which can be determined from the oscillator model, should be maintained throughout growth and under variable environmental conditions.

Energetics and cost of locomotion

The power required to operate the oscillator is negligibly small compared with the power required to form the jets. The distribution of the power output during the closing phase for *Placopecten magellanicus* (Fig. 7D) agrees well with that for *Argopecten irradians* (Fig. 4 in Marsh *et al.* 1992). The main difference is that our curve does not show an initial peak before the major peak. One possible reason for this disparity is that our kinematic data were collected at a lower time resolution than that of Marsh *et al.* (1992) and that this transient phenomenon has not been detected. However, calculation of the power output by Marsh *et al.* (1992) is fairly crude at the initial part of the closing phase. This is because the velum around the valve is not completely sealed during the initial closing phase, and this results in a large exit opening spread around the edge of the valve. The local fluid pressure they measured near the adductor muscle will not adequately characterize the pressure field in the whole cavity at this stage, because the fluid pressure near the periphery is close to the ambient pressure. Hence, the power calculated as the flow rate multiplied by the pressure measured at one point in the cavity is inappropriate, as pointed out above, and would result in an overestimate of the initial calculated power. In fact, the initial peak of Marsh *et al.* (1992) is almost masked by the amount of noise in their curve. A larger initial peak of the *in vitro* power output of the adductor muscle was obtained by Marsh and Olson (1994). They attributed it to requirements to accelerate the added mass and to compress the hinge ligament. The more complete analysis of the dynamics of the locomotor system presented in the present paper shows that the force and power required to move the shell-hinge/outer-fluid subsystem are far smaller than the values corresponding to the initial peak on the *in vivo* or *in vitro* power curves of these previous studies.

Fairly good agreement was found between the scallop adductor muscle *in vivo* power output and *in vitro* data replicating the *in vivo* strain cycle on isolated muscle fibres (Marsh and Olson, 1994). Except for the initial peaks, this agreement in power output was found even between different species and perhaps different swimming situations. This implies that the power output obtained from the *in vitro* work-loop measurements can give useful predictions for *in vivo* performance. However, the force behaviour of the *in vitro* work-loop measurements was found to be quite different from that of the *in vivo* results; this will be addressed elsewhere.

We did not record the mass of the adductor muscle (or its striated part) for the animals filmed. In order to compare our results with those of other studies, the approximate mass of the striated muscle of the 0.065 m long *Placopecten magellanicus* can be estimated. The valve mass and the total mass can be taken as 18.21×10^{-3} kg and 35.91×10^{-3} kg, respectively, from Dadswell and Weihs (1990). The mass of wet soft tissues is then 17.7×10^{-3} kg. The mass of the wet muscle is about half of that of the total wet tissues (Morton, 1980), and the ratio of the striated part to total muscle is approximately 0.815 (Gould, 1971). Thus, the wet striated muscle mass is approximately 7.21×10^{-3} kg.

The peak power, average power and cyclic work per unit mass for the 0.065 m long individual filmed (ang32) are listed in Table 5. The results for *Argopecten irradians* and *Chlamys hastata* are also given (Marsh *et al.* 1992). The peak power for *P. magellanicus* is higher than the average values for

Argopecten irradians and *Chlamys hastata*, but the cyclic work is lower than their average values. In general, a muscle performs less work in each contraction when a higher power output is needed (Alexander, 1992). The $9\,J\,kg^{-1}$ work that the muscle of our filmed individual was doing is lower than the value of $20\,J\,kg^{-1}$ suggested by Alexander (1992), although an even lower value of $7\,J\,kg^{-1}$ has been reported for the starling *Sturnus vulgaris* (Biewener *et al.* 1992). However, we believe that the mass of the striated muscle is likely to be an overestimate. In this case, the values for the muscle energetic quantities per unit mass will be higher.

The rate of oxygen consumption has frequently been measured to estimate the cost of swimming for both jet-propelled animals (Daniel, 1985; Webber and O'Dor, 1986) and fishes (Brett, 1964; Webb, 1971; Videler, 1993). The cost of transport for squid *Illex illecebrosus* was found to be about three times that for sockeye salmon *Oncorhynchus nerka*, and the efficiency of locomotion for fish was about three times that for squid (Webber and O'Dor, 1986). Their work did not estimate the energy required to power the movement of the mantle and the external fluid, and the jet power was considered to account for the entire power output of the muscle. It is not known how the energy generated by muscle contraction during swimming in squid is partitioned into the two basic components, the hydrodynamic power for the jet and the power required to accomplish the pumping cycle. DeMont and Gosline (1988) carried out a more complete investigation on the energetics of jellyfish swimming, although the external fluid reaction was still omitted. They found that the total mechanical power was spent as follows: 39–61 % on the jet, 19–32 % on the kinetic energy of the bell and 20–29 % on the deformation of the bell.

From Table 4, the mechanical work done by the muscle on the oscillator, i.e., the pumping structure, is 0.502×10^{-3} J and the total muscle work done in one cycle is 64.8×10^{-3} J. The ratio of the work done on the oscillator to the total work is therefore about 0.007 and the former can almost be ignored in the energy budget. This means that more than 99 % of the mechanical energy from the muscle is spent on jet production, which is basically the hydrodynamic power of the jet. Thus, the Froude efficiency (Alexander, 1977) of the pulsed jet propulsion approximates the mechanical efficiency of the locomotor system. This could be a fundamental advantage for the jet-propelled scallop. It has been known that the Froude efficiency for jet-propelled animals is generally much lower than that for most axial undulatory propulsion in fishes. Our recent results (Cheng and DeMont, 1996*b*) show that Froude efficiency for scallops (*Placopecten magellanicus*) decreases during growth from 0.5 to 0.3 for level swimming, and from about 0.4 to 0.2 for climbing at an angle of 25 °. However, fishes may need a relatively higher proportion of the mechanical power available from the muscles to supply the kinetic energy for the undulation of their body (particularly for anguilliform and subcarangiform fishes) and the strain energy to deform the body tissues (Wainwright, 1983; Cheng *et al.* 1994; Cheng and Blickhan, 1994; Bowtell and Williams, 1994). Integrated energetic studies will certainly serve as a valuable approach to provide more information on the locomotor mechanism and the energy flow from the output of the muscle to the useful hydrodynamic propulsive work in aquatic animals. Comparative studies on other jet-propelled animals and fishes may help us to understand how jet-propelled animals with a low Froude efficiency survive and compete with fishes in the open ocean.

List of symbols

A_j	cross-sectional area of the jet at exit
A_v	area of the valve projected on the commissural plane
A_m	cross-sectional area of the adductor
A_{mq}	cross-sectional area of the fast part of the adductor
c	effective viscous coefficient due to hinge and outer fluid reaction
c_f	rotational viscous coefficient of pseudo-viscosity due to outer fluid reaction
c_h	rotational viscous coefficient of hinge
F	jet thrust
F_{fi}	total force due to the inner fluid pressure
$F_{fi\beta}$	coefficient defined in equation 10
f	clapping frequency
I	effective inertial moment due to hinge and outer fluid reaction
I_f	added moment inertia of one shell
I_v	inertial moment of half of the two-valve mass
k	effective stiffness due to hinge and outer fluid reaction
k_f	rotational pseudo-stiffness due to outer fluid reaction
k_h	rotational stiffness of hinge
L_m	muscle length at any instant of time
L_{mc}	muscle length when valves are closed
L_{mo}	muscle length at maximum valve opening
M_{fe}, M_h, M_v	moment about the hinge for external fluid force, for hinge deformation or for valve inertia, respectively
M_{fi}	moment about the hinge due to the inner fluid pressure
$M_{fi\beta}$	coefficient of internal flow moment, defined in equation 12
M_m	total moment generated by muscle contraction
M_{mo}, M_{mj}	muscle moment used for the oscillator, muscle moment for the jet flow, respectively
P_d	rate of energy dissipation by the effective damping
P_e	rate of change of strain energy stored in the effective spring
P_k	rate of change of kinetic energy for scallop shell mass and added mass
P_m	total power generated by muscle contraction
P_{mo}, P_{mj}	power spent on the oscillator, or power spent

	on the jets, respectively
P_{mj0}, P_{mj1}	jet power due to uniform pressure and variable pressure, respectively
p_i	effective pressure at inner surface of shell
$p_{i\beta}$	coefficient defined in equation 8
p_j, p_s	inner fluid pressure at exit, or at shell, respectively
S_L	shell height (see Fig. 2)
S_x	*x*-coordinate of any point on the shell
T	time for one jet cycle
t	time
t_m	thickness of aerofoil
t_s	thickness of two shells
U	swimming speed
U_j, U_s	fluid velocity at exit, or at the shell, respectively
V_e	volume of expellable water at any instant
V_m	volume occupied by the adductor muscle
V_s	volume enclosed by the wedge bounded by the velum and two shell planes
W_m	total work done by the muscle during one cycle
W_{mo}, W_{mj}	work done on the oscillator, or work done on the jets, respectively
α	angle of attack
α_T	trajectory angle between the swimming direction and horizontal surface
β_{min}, β_{max}	minimum and maximum half-gape angle, respectively
β_{mm}	effective maximum half-gape angle
$\beta(t)$	half-gape angle
γ_{min}, γ_{max}	minimum and maximum gape angles, respectively
$\gamma(t)$	angular displacement of the hinge
Δt_o, Δt_c, Δt_g	duration of opening, closing or gliding phase, respectively
ε	muscle strain
ε_0	maximum muscle strain
ε_1	coefficient defined in equation 30
λ_{to}, λ_{tc}, λ_{tg}	ratio of time interval of opening, closing or gliding phase to one cycle, respectively
λ_1, λ_2	geometrical parameter (see Fig. 2)
$\lambda_A=1-(A_m/A_v)$, $\lambda_{Aj}=A_j/A_v$	area ratios
ρ	density of sea water
σ	muscle stress
σ_{mm}	coefficient of muscle stress

We thank K. Bryden for assisting in the film analysis, C. Leger for writing the data collection software and J. Carmichael, J. Flynn and C. McConnell (St. F. X.) for their comments on the manuscript. We also thank Dr E. Kenchington (DFO, Halifax) for supplying the scallops, and the Department of Physical Education, Dalhousie University, for the loan of the high-speed cine equipment. J.-Y.C. was supported by an NSERC (Canada) International Fellowship. The research was funded by grants from NSERC (Canada) and ACOA (Interim Funding Research Project) to M.E.D.

References

ALEXANDER, R. MCN. (1966). Rubber-like properties of the inner hinge-ligament of Pectinidae. *J. exp. Biol.* **44**, 119–130.

ALEXANDER, R. MCN. (1977). Swimming. In *Mechanics and Energetics of Animal Locomotion* (ed. R. McN. Alexander and G. Goldspink), pp. 222–247. London: Chapman & Hall.

ALEXANDER, R. MCN. (1992). The work that muscle can do. *Nature* **357**, 360–361.

BEDDOW, T. A., VAN LEEUWEN, J. L. AND JOHNSTON, I. A. (1995). Swimming kinematics of fast starts are altered by temperature acclimation in the marine fish *Myoxocephalus scorpius*. *J. exp. Biol.* **198**, 203–208.

BIEWENER, A. A., DIAL, K. P. AND GOSLOW, G. E. (1992). Pectoralis muscle force and power output during flight in the starling. *J. exp. Biol.* **164**, 1–18.

BLICKHAN, R. AND CHENG, J.-Y. (1994). Energy storage by elastic mechanisms in the tail of large swimmers – a re-evaluation. *J. theor. Biol.* **168**, 315–321.

BOWIE, M. A., LAYES, J. D. AND DEMONT, M. E. (1993). Damping in the hinge of the scallop *Placopecten magellanicus*. *J. exp. Biol.* **175**, 311–315.

BOWTELL, G. AND WILLIAMS, T. L. (1994). Anguilliform body dynamics: a continuum model for the interaction between muscle activation and body curvature. *J. math. Biol.* **32**, 83–91.

BRETT, J. R. (1964). The respiratory metabolism and swimming performance of young sockeye salmon. *J. Fish Res. Bd Can.* **21**, 1183–1226.

CHENG, J.-Y. AND BLICKHAN, R. (1994). Bending moment distribution along swimming fish. *J. theor. Biol.* **168**, 337–348.

CHENG, J.-Y. AND DEMONT, M. E. (1996*a*). Hydrodynamics of scallop locomotion: unsteady fluid forces on clapping shells. *J. Fluid Mech.* **317**, 73-90.

CHENG, J.-Y. AND DEMONT, M. E. (1996*b*). Jet-propelled swimming in scallops: swimming mechanics and ontogenic scaling. *Can. J. Zool.* (in press).

CHENG, J.-Y., PEDLEY, T. J. AND ALTRINGHAM, J. D. (1994). A continuous dynamic model for fish swimming. In *Proceedings of the Second World Congress of Biomechanics* (ed. L. Blankevoort and T. G. M. Kooloos), p. 196. (abstract). Nijmengen: Stichting World Biomech.

CHENG, J.-Y., ZHUANG, L.-X. AND TONG, B.-G. (1991). Analysis of swimming three-dimensional waving plates. *J. Fluid Mech.* **232**, 341–355.

DADSWELL, M. J. AND WEIHS, D. (1990). Size-related hydrodynamic characteristics of the giant scallop *Placopecten magellanicus* (Bivalvia: Pectinidae). *Can. J. Zool.* **68**, 778–785.

DANIEL, T. L. (1985). Cost of locomotion: unsteady medusan swimming. *J. exp. Biol.* **119**, 149–164.

DANIEL, T. L., JORDAN, C. AND GRUNBAUM, D. (1992). Hydromechanics of swimming. In *Advances in Comparative and Environmental Physiology*, vol. 11 (ed. R. McN. Alexander), pp. 17–49. Berlin: Springer-Verlag.

DEMONT, M. E. (1990). Tuned oscillations in the swimming scallop *Pecten maximus*. *Can. J. Zool.* **68**, 786–791.

DEMONT, M. E. AND GOSLINE, J. M. (1988). Mechanics of jet propulsion in the hydromedusan jellyfish *Polyorchis penicillatus*. II. Energetics of the jet cycle. *J. exp. Biol.* **134**, 333–345.

FUNG, Y. C. (1993). *Biomechanics: Mechanical Properties of Living Tissues*. New York: Springer-Verlag.

GOULD, S. J. (1971). Muscular mechanics and the ontogeny of swimming in scallops. *Paleontology* **14**, 61–94.

GRUFFYDD, L. D. (1976). Swimming in *Chlamys islandica* in relation

to current speed and an investigation of hydrodynamic lift in this and other scallops. *Norw. J. Zool.* **24**, 365–378.

HARPER, D. G. AND BLAKE, R. W. (1989). On the error involved in high-speed film when used to evaluate maximum accelerations of fish. *Can. J. Zool*. **67**, 1929–1936.

HAYAMI, I. (1991). Living and fossil scallop shells as airfoils: an experimental study. *Paleobiology* **17**, 1–18.

LIGHTHILL, M. J. (1975). *Mathematical Biofluiddynamics*. Philadelphia: SIAM.

MADIN, L. P. (1990). Aspects of jet propulsion in salps. *Can. J. Zool*. **68**, 765–777.

MARSH, R. L., OLSON, J. M. AND QUZIK, S. K. (1992). Mechanical performance of scallop adductor muscle during swimming. *Nature* **357**, 411–413.

MARSH, R. M. AND OLSON, J. M. (1994). Power output of scallop adductor muscle during contractions replicating the *in vivo* mechanical cycle. *J. exp. Biol*. **193**, 136–156.

MOORE, J. D. AND TRUEMAN, E. R. (1971). Swimming of the scallop, *Chlamys opercularis* (L.). *J. exp. mar. Biol. Ecol*. **6**, 179–185.

MORTON, B. (1980). Swimming in *Amusium pleuronectes* (Bivalvia: Pectinidae). *J. Zool., Lond.* **190**, 375–404.

O'DOR, R. K. (1988). The force acting on swimming squid. *J. exp. Biol*. **137**, 421–442.

OLSON, J. M. AND MARSH, R. L. (1993). Contractile properties of the striated adductor muscle in the bay scallop *Argopecten irradians* at several temperatures. *J. exp. Biol*. **176**, 175–193.

THOMSON, W. T. (1988). *Theory of Vibration with Applications*. Englewood Cliffs: Prentice Hall.

TRUEMAN, E. R. (1975). *The Locomotion of Soft-bodied Animals*. London: Edward Arnold.

VIDELER, J. J. (1993). *Fish Swimming*. London: Chapman & Hall.

VOGEL, S. (1985). Flow-assisted shell reopening in swimming scallops. *Biol. Bull. Mar. biol. Lab., Woods Hole* **169**, 624–630.

WAINWRIGHT, S. A. (1983). To bend a fish. In *Fish Biomechanics* (ed. P. W. Webb and D. Weihs), pp. 68–91. New York: Praeger.

WEBB, P. W. (1971). The swimming energetics of trout. II. Oxygen consumption and swimming efficiency. *J. exp. Biol*. **55**, 521–540.

WEBBER, D. M. AND O'DOR, R. K. (1986). Monitoring the metabolic rate and activity of free-swimming squid with telemetered jet pressure. *J. exp. Biol*. **126**, 205–224.

WEIHS, D. (1977). Periodic jet propulsion of aquatic creatures. *Fortschr. Zool*. **24**, 171–175.

WOLTRING, H. J. (1986). A Fortran package for generalized, cross-validatory spline smoothing differentiation. *Adv. Eng. Software* **8**, 104–113.